

See discussions, stats, and author profiles for this publication at: <https://www.researchgate.net/publication/254516325>

Fluidized-Bed Combustion of Mixtures of Rapeseed Cake and Bark: The Resulting Bed Agglomeration Characteristics

ARTICLE in ENERGY & FUELS · APRIL 2012

Impact Factor: 2.79 · DOI: 10.1021/ef300130e

CITATIONS

16

READS

34

8 AUTHORS, INCLUDING:



Alejandro Grimm

Swedish University of Agricultural Sciences

17 PUBLICATIONS 413 CITATIONS

[SEE PROFILE](#)



Dan Boström

Umeå University

136 PUBLICATIONS 1,980 CITATIONS

[SEE PROFILE](#)



Mikko Markus Hupa

Åbo Akademi University

426 PUBLICATIONS 5,476 CITATIONS

[SEE PROFILE](#)

Fluidized-Bed Combustion of Mixtures of Rapeseed Cake and Bark: The Resulting Bed Agglomeration Characteristics

Patrycja Piotrowska,^{*,†} Alejandro Grimm,[§] Nils Skoglund,[‡] Christoffer Boman,[‡] Marcus Öhman,[§] Maria Zevenhoven,[†] Dan Boström,[‡] and Mikko Hupa[†]

[†]Process Chemistry Centre, Laboratory of Inorganic Chemistry, Åbo Akademi University, Turku, Finland

[‡]Energy Technology and Thermal Process Chemistry, Umeå University, Umeå, Sweden

[§]Department of Engineering Sciences & Mathematics, Energy Engineering, Luleå University of Technology, Luleå, Sweden

ABSTRACT: The bed agglomeration characteristics resulting from the combustion of 11 mixtures of rapeseed cake and spruce bark were studied in a bench-scale bubbling fluidized-bed reactor (5 kW). The objective was to determine the defluidization temperatures and the prevailing bed agglomeration mechanism as functions of the fuel mixture. Controlled fluidized-bed agglomeration tests were performed for each mixture with quartz sand as the bed material. The total defluidization temperatures and the initial defluidization temperatures were determined based on the measured pressure and temperature profiles in the bed. After combustion, bottom ash samples, agglomerates, and fly ash samples were analyzed by means of scanning electron microscope combined with energy dispersive X-ray detector (SEM-EDX). The composition of the ash-forming matter produced by the combustion of rapeseed cake is significantly different from that produced by the combustion of bark, resulting in different bed agglomeration tendencies. Bark contains ash-forming matter dominated by calcium, with some silicon and potassium, whereas rapeseed cake is rich in phosphorus, potassium, and sodium. The total defluidization temperature for pure bark was above 1045 °C, whereas, for rapeseed cake, defluidization occurred during combustion (800 °C). During the combustion of bark, the formation of a potassium-rich layer on the silica-bed grains was found to be a crucial for the formation of agglomerates. The low defluidization temperature for the rapeseed cake can be attributed to the formation of sticky ash, which is dominated by phosphates. Two main phosphate forms were observed in the neck between the silica grains: calcium–potassium/sodium phosphates, and magnesium–potassium phosphates. As the proportion of bark increased, the Ca/P ratio increased in the fuel mixture, and the formation of high-temperature melting phosphates in the ash was favored. However, the addition of bark also favored the formation of a potassium-rich layer on the silica bed material, leading to the coexistence of both bed agglomeration mechanisms. In the present work, mixtures with a minimum of 60 wt % bark resulted in significantly increased defluidization temperatures and reduced bed agglomeration tendencies, compared to what occurs in rapeseed cake monocombustion.

1. INTRODUCTION

In the power industry, fossil fuels are currently being replaced with biomass in an attempt to decrease CO₂ emissions. However, caution should be exercised in the industrial implementation of new biomass fuels, since they can create new challenges when fired. Biomass fuels differ significantly from coal in terms of the chemical composition of ash-forming matter.^{1–6} This may have a crucial impact on fuel ash behavior and the suitability of a fuel for combustion processes.^{6–12} The co-combustion of fuel mixtures can be especially challenging,⁹ since the ash-related problems often are dependent nonlinearly on the proportions of the two fuels in the mixture.¹³

Recently, more attention has been paid to agricultural biomass; such materials are rich in phosphorus. The combustion behavior of fuels rich in phosphorus differs from that of woody fuels.^{8,14–19} As Boström et al.¹⁴ found, phosphate compounds exhibit high stability during combustion. Furthermore, phosphorus shows a strong affinity for basic cations (e.g., potassium) than silicon¹⁴ and is the main element controlling ash transformation reactions.¹⁶

Piotrowska et al.¹⁷ determined that ~70% of the total phosphorus in rapeseed cake is organically associated. According to biological studies,²⁰ this fraction may be correlated with phosphorus bound in salts of phytic acid

(myo-inositol hexaphosphate) and its degradation products (mainly inositol pentaphosphate). The release mechanism of phosphorus and potassium from the inositol phosphate complex was studied by Hao et al.,¹⁹ in the context of the combustion of bran. They suggested that this complex decomposes to KPO₃, which melts at ~800 °C.¹⁵

Fluidized-bed combustion (FBC) is considered to be a flexible technology, suitable for the combustion of fuels of varying quality. However, the operation of fluidized beds is limited by the tendency of bed particles to agglomerate, leading to defluidization.²¹ Different fuels have different agglomeration tendencies, depending on the ash composition, so when new fuels are considered, it is important to determine the agglomeration tendency.

Agglomeration during the (co)combustion of biomass fuels has been studied by several groups.^{21–31} The terms “agglomeration” and “bed sintering” are used interchangeably to describe the same phenomenon. Sintering is defined as the formation of bonds between particles at elevated temperatures,³² while agglomeration is defined as the formation of

Received: January 22, 2012

Revised: March 1, 2012

Published: March 1, 2012



clusters of bonded primary particles, called “agglomerates”. The agglomeration of bed material in a fluidized-bed reactor at high temperatures involves the sintering of bed material grains.

Sintering mechanisms have been extensively studied in materials science, since most bulk ceramic components and glasses are made by sintering compressed powder.³² The same mechanisms apply to the sintering of ashes and bed material in fluidized-bed combustors. Skrifvars et al.³³ described three different mechanisms responsible for the sintering of ash in fluidized beds: partial melting; partial melting with a viscous liquid (also known as viscous flow sintering); and gas–solid chemical reactions. Partial melting refers to sintering via the appearance in fuel-derived ash particles of a liquid phase consisting of molten salts. The amount of liquid phase controls the ash stickiness and is considered to be the controlling parameter for agglomerate formation. This type of bed sintering is also called melt-induced agglomeration³⁴ or direct adhesion of bed material grains by molten particles.³⁵ The influence of char burnout on the formation of molten phases was studied by Lin et al.²³ and Scala et al.^{29,36} They suggested that the temperature of burning char particles might be higher than that of the average bed temperature, resulting in melt formation.

Both partial melting and partial melting with viscous flow involve the occurrence of a liquid phase, but the latter arises in the context of silicate system. Silicon can form highly polymerized silicate networks; their melt may have high viscosity in contrast to salt melts, which have low viscosity. A highly viscous liquid can form either on the fuel ash particles (in pulverized coal combustion) or on the bed material (when silica sand is used). The first mechanism involves the formation of highly viscous melt originating from fuel-derived ash. The second involves the interactions of the released inorganic compounds with the bed material, leading to the formation of a layer on the silica grains via different mechanisms.²² Depending on its composition, the layer could be the sticky prerequisite for the formation of agglomerates.²⁶ This type of bed sintering is referenced by Visser et al.³⁴ as “coating-induced agglomeration”. They concluded that the initial composition of the coating layer, which is dependent on both the fuel ash composition and ash bed material interaction processes, is an important parameter for bed sintering.

The third sintering mechanism described by Skrifvars et al.³³ is gas–solid interaction, also known as “chemical reaction sintering”. These interactions have been studied extensively in the context of deposit formation in the convective pass of a boiler. However, chemical reactions of gaseous species (e.g., alkali metals) with the bed material have also been shown to occur in fluidized beds, and reaction product layers have been found on grain surfaces.^{22,25,30,34} The product layers are distinguished based on composition, and the potassium-rich innermost layer is referred to as the inner reaction layer.^{16,25,27} Depending on its composition, this layer could be partly molten and so could lead to viscous flow bed sintering.

A different perspective on the formation of agglomerates is proposed by De Geyeter,³⁷ who suggested two pathways leading to bed sintering: without active layer formation and with active layer formation. The first describes the formation of agglomerates when no chemical interaction takes place between the bed material grain and the molten fuel ash; the second identifies the chemical interaction between bed grains and ash as an important mechanism underlying bed sintering.

Despite the different perspective on agglomeration mechanisms in biomass FBC, there is universal agreement that alkali

metals play a significant role in the formation of agglomerates.^{22,26} However, recently, the focus has shifted to phosphorus, since it can aggravate bed agglomeration.^{10,17,16,31}

Piotrowska et al.¹⁷ found that, during the co-combustion of wood and rapeseed cake, the formation of low-melting potassium silicates on the surface of the bed material grains may be followed by the adhesion of phosphorus-rich molten ash particles, which can result in agglomerate formation during FBC at 850 °C. Grimm et al.¹⁶ investigated bed agglomeration characteristics during the FBC of phosphorus-rich biomass and concluded that the direct adhesion of partly molten ash particles containing K–Mg–P and Ca–K–Mg–P to the bed material grains is the dominant process. However, whether the presence of phosphorus aggravates agglomeration is strongly dependent on the Ca/P ratio. The addition of limestone^{15,17,19,31,38} was found to be beneficial, because it prevents the formation of a potassium silicate layer on bed material grains³¹ and increases phosphorus retention in the bed, most probably through the formation of calcium phosphates. Consequently, some gaseous potassium could be released.¹⁹

Although the co-combustion of bark and phosphorus-rich biomass has been investigated,^{39,40} there are no systematic studies of well-defined mixtures. The objective of the present work was to investigate the co-combustion of well-defined mixtures of rapeseed cake (RC), which is a phosphorus-rich fuel, and spruce bark, which is a calcium-rich fuel. The defluidization temperatures were determined, and the dominant agglomeration mechanisms for different fuel mixtures were identified. Eleven different mixtures were prepared, having increasing proportions of bark (0–100 wt %). Controlled fluidized-bed agglomeration tests⁴¹ were performed in a bench-scale bubbling fluidized-bed reactor (5 kW) in which quartz sand (200–250 μm) was used as the bed material. After combustion, bottom ash samples, agglomerates, and fly ash samples were studied by means of scanning electron microscope combined with energy dispersive X-ray detector (SEM-EDX), and the bed agglomeration mechanism was inferred from the results.

2. EXPERIMENTAL METHODS

2.1. Fuels. Experiments were conducted using two fuels: spruce bark (from the Södra Cell plant at Mönsterås Bruk, Sweden) and rapeseed cake (from Emmelev A/S, Denmark). The samples were ground, and 11 different mixtures were prepared, with the proportion of bark ranging from 0 to 100 wt %. For each mixture, ~40 kg of ground material was homogenized in a concrete mixer before pelletizing. The pellets were 8 mm in diameter and <150 mm in length (~50–150 mm), and the moisture content was ~10–12 wt %. Fuel analysis was performed for the rapeseed cake (RC) and bark by an accredited external laboratory according to Swedish standards. The composition of the mixtures was calculated based on the compositions of the original fuels.

2.2. Reactor. The experiments were conducted in a bench-scale 5 kW bubbling fluidized-bed reactor (BFB), described in detail by Öhman and Nordin.⁴¹

The stainless steel reactor is 2 m high, with an inner diameter of 100 mm in the bed section and of 200 mm in the freeboard section. The maximum temperature that can be reached is 1045 °C (in the bed). A constant temperature is achieved using preheated primary air, in conjunction with electrical heaters in the freeboard section. A perforated stainless steel plate at the bottom of the fluidized bed with the total open area of 1% functions as an air distributor. In the experiments, the reactor was used as a combustor and subsequently for controlled fluidized-bed agglomeration tests. During the agglomeration tests, propane was burned below the air distribution plate, making it

possible to achieve the desired mixing of gases and to maintain a combustion atmosphere in the reactor. The temperature and pressure drop in the bed were continuously monitored using two thermocouples and two pressure probes.

2.3. Experiments. The experimental matrix consisted of 11 experiments, each of which had two stages: combustion and agglomeration (see Figure 1).

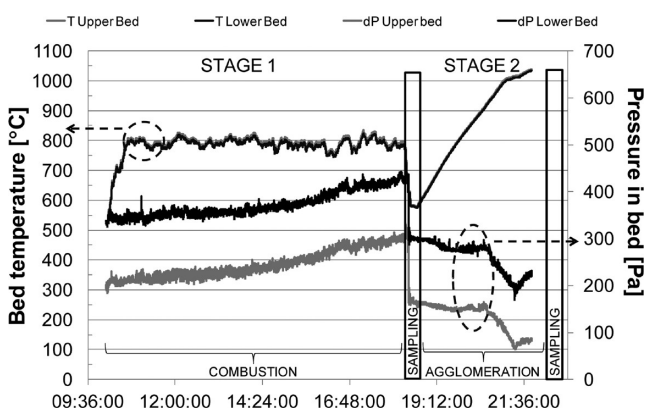


Figure 1. Stages in controlled agglomeration test: bed temperature and pressure versus time for 90 wt % bark and 10 wt % rapeseed cake (RC).

During the first stage, ~4–5 kg of fuel mixture, continuously fed into the reactor with a screw feeder, was burned for 8 h at 800 °C. Bark and rapeseed cake have a similar energy content, so a constant fuel input guaranteed a constant energy output of 3.3 ± 0.3 kW. For each experimental run, 540 g of fresh quartz sand (>98% SiO₂) was used, with an initial particle size in the range of 200–250 µm. The excess oxygen level was maintained at 8% dry flue gas for all the experiments, and the air flow was kept constant at 80 NL/min. During the combustion phase, the fluidization velocity was kept 10 times higher than the minimum fluidization velocity, corresponding to ~1 m/s. After 8 h of combustion, the fuel feed was stopped, and a sample of the bed material was collected. The air flow was minimized to 30 NL/min, and the combustion of propane gas in a chamber below the primary air distributor plate was initiated. The bed then was heated at a constant rate of 3 °C/min until defluidization was achieved.

2.4. Initial and Total Defluidization. The recorded temperature and pressure curves were analyzed to determine the initial and the total defluidization temperatures. The initial defluidization temperature is the temperature at which changes in the bed pressure are first observed, and it probably indicates that the growth of agglomerates and/or slagging begin to occur. In the case where the pressure curves were constantly declining during the 8-h combustion stage, initial defluidization was said to occur during combustion. When the pressure curves were stable or increasing during the combustion stage, the initial defluidization temperature was determined based on the pressure curves for the agglomeration stage: it is defined as the point of intersection of two tangent lines to the differential pressure curves. The total defluidization temperature refers to the temperature at which no fluidization is observed: it is defined as the first temperature at which the pressure curve reaches its minimum (Figure 2).

2.5. Samples and Analyses. In addition to studying fuel samples, this work analyzed bottom ash samples, which are known to consist mainly of particles originating from bed material and some fuel-derived ash particles.⁴² Two bottom ash samples were collected during each experimental run: one after the combustion stage, and the other after the agglomeration test. Both the formation of layers on silica bed grains and the formation of agglomerate necks (necks formed between silica bed grains) were examined by means of SEM/EDX. For this purpose, the samples were embedded in epoxy and ground with SiC grinding paper having four different grain sizes, ranging from 320 to 2500, until a smooth-surfaced cross section was obtained; no liquid

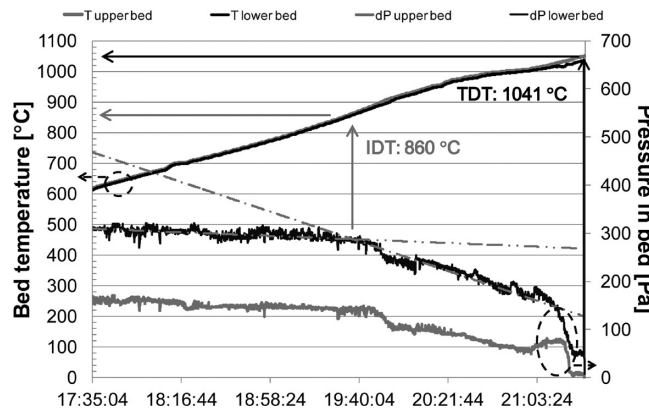


Figure 2. Bed defluidization temperatures indicated on the temperature and pressure profile for 60 wt % bark and 40 wt % rapeseed cake (RC).

agent was used during polishing. Next, the samples were coated with carbon to enable SEM/EDX analysis, and magnifications of 200× and higher were used to study the composition of layers and agglomerate necks.

In addition, fly ash samples were taken from the cyclone ($d_p < 10$ µm), and their overall composition was studied by means of SEM/EDX. For this purpose, ash samples were mounted on carbon tape and covered with a thin carbon layer, and then area analyses were performed at magnifications of 30× and 50×.

The SEM/EDX instrument used was a LEO Gemini 1530 system with a Thermo Scientific UltraDry Silicon Drift Detector (SDD). The vacuum in the SEM chamber was $\sim 10^{-6}$ mbar.

2.6. Bed Particle Layer Thickness. The bottom ash samples (see section 2.5) taken after the combustion stage but before agglomeration were also used to study the total thickness of the layer on the bed particle grains. Twelve (12) randomly chosen pictures were taken at a magnification of 100× and analyzed with MeasureIT software (Olympus Soft Imaging Solutions GMBH). The layer thickness was measured equidistantly at ~10–15 sites around the particle (Figure 3). Approximately 30 particles were studied for each experiment, and the data were used to draw a cumulative distribution for each mixture.

3. RESULTS AND DISCUSSION

3.1. Fuel Properties and Ash-Forming Matter. The standard fuel analyses (proximate and ultimate) are shown in Table 1. Both fuels have similar heating values, resulting in a similar energy output, which is independent of the mixture fired. However, they differ substantially in terms of fixed carbon and ash content. Bark has nearly 50% more fixed carbon (~23 wt % db) than rapeseed cake (RC), while RC has twice the amount of ash. The ultimate analyses revealed substantial differences in the N, S, and Cl contents of the two fuels. These elements are present in RC in high concentrations (4.9 wt % db N, 0.5 wt % S, and 0.7 wt % Cl), whereas in bark, they are below the detection limits.

Table 2 shows the ash composition and the calculated proportion of bark ash in the total fuel ash from each mixture; the latter indicates that the fuel ash compositions of mixtures containing up to 50 wt % bark are dominated by RC ash and may have similar properties. The fuel mixture containing 60 wt % bark (B60) contains approximately equal amounts of fuel ash originating from RC and from bark. The composition of the ash-forming matter in bark is dominated by calcium, silicon, and potassium, whereas the ash-forming matter in RC is dominated by phosphorus and potassium, along with some calcium and sulfur. In addition, in RC, the sodium content is high, compared to that found in rapeseed meal.³⁹ The

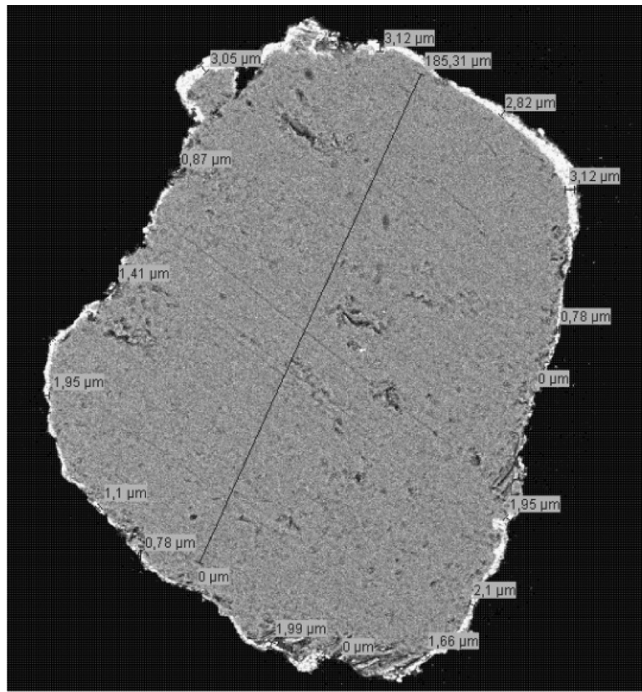


Figure 3. Example of the measurement of the layer thickness on a bed material particle from the combustion of 30 wt % bark and 70 wt % rapeseed cake (RC).

composition of these mixtures can result in the formation of ash with a low first melting point,^{15,43} and it may be the reason for ash-related problems during combustion.

3.2. Composition of FBC Fly Ash Samples. The composition of the fly ash samples is shown in Figure 4. As the proportion of bark increases, the phosphorus and alkali-metals content decreases in the ash particles, whereas the total amount of calcium compounds increases. The results of the analysis are in a good agreement with the composition of the total fuel ash, confirming that the mixtures were well-prepared. As the proportion of bark increases, the Ca/P molar ratio increases from 0.9 to 18.3. For the mixture with 60 wt % bark, the Ca/P molar ratio is 2.03. This large amount of Ca could favor the formation of calcium phosphate compounds having higher melting temperatures than alkali-metal phosphates.¹⁵ In the fly ash sample, the amount of sulfur was slightly higher for mixtures with 60 and 70 wt % bark. The addition of sulfur to

biomass fuels with high potassium content has a positive effect on the defluidization temperature during fluidized bed combustion, as determined by De Geyter et al.³⁷ If there was any chlorine present in the fly ash, the amount was <5 mol %. The Cl/S molar ratio was high, ranging from 0.47 to 0.65 for mixtures with 20 to 100 wt % of bark. Ratios over 0.5 indicate a high tendency for deposit formation.⁴⁴

3.3. Thickness of the Layer on Bed Material Particles before the Agglomeration Stage. Comparisons of the layers formed during the combustion of each fuel separately and mixtures of the two fuels revealed significant differences. When 100 wt % rapeseed cake was combusted, discontinuous layers formed and they resembled lumps of ash particles glued to the surface of the bed material particles. In contrast, during the combustion of bark, a continuous layer formed around the bed material particles, within which two different layers could be distinguished: homogeneous inner reaction layer, and outer coating layer exhibiting a granular structure.

In the case of the fuel mixtures, varying combinations of the different layer phenomena were observed: discontinuous layer (or absence of layer), continuous layer with uniform thickness, and continuous layer with nonuniform thickness. Figure 5 shows the cumulative distribution of the total layer thickness on the particles for the different fuel mixtures; Figure 6 shows the arithmetic mean and median for these distributions.

For rapeseed cake combustion, most of the data lies in the range 0–0.3 μm, whereas, for bark combustion, continuous layers formed, evenly distributed in the range of 1–4 μm. The mixtures were categorized into two main groups based on two critical coating thicknesses 1 and 2 μm. The first group has discontinuous layers or none at all, with more than 20% of the measurements below 1 μm and more than 60% of the measurements below 2 μm. The second group is characterized by a continuous layer on the particles, with less than 20% of the measurements below 1 μm, and less than 60% below 2 μm. The distribution for the fuel mixture with 50 wt % bark lies between these two groups. Figure 6 shows the distribution of the measurement data. The median exhibits an increasing trend with an increasing proportion of bark. For 100 wt % bark, the uniform thickness of the coating is indicated by the low variation between the arithmetic mean and the median values.

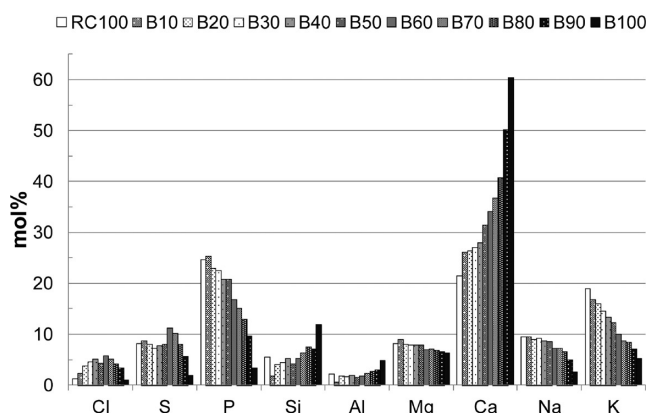
Statistical analysis is widely applied for modeling of various processes in industrial furnaces, e.g., to control chemical composition during steel making.⁴⁵ However, in this paper, a

Table 1. Fuel Properties

	RC	10 wt % bark	20 wt % bark	30 wt % bark	40 wt % bark	50 wt % bark	60 wt % bark	70 wt % bark	80 wt % bark	90 wt % bark	bark
lower heating value, LHV (MJ/kg db)	20.6	20.5	20.4	20.4	20.3	20.2	20.1	20.0	20.0	19.9	19.8
proximate analysis (wt % db)											
volatile matter	77.8	77.3	76.7	76.2	75.6	75.1	74.5	74.0	73.4	72.9	72.3
fixed carbon	14.7	15.5	16.3	17.1	17.9	18.8	19.6	20.4	21.2	22.0	22.8
ash content	7.5	7.2	7.0	6.7	6.5	6.2	5.9	5.7	5.4	5.2	4.9
ultimate analysis (wt % db)											
C	50.0	50.2	50.5	50.7	50.9	51.2	51.4	51.6	51.8	52.1	52.3
H	6.6	6.5	6.4	6.3	6.2	6.2	6.1	6.0	5.9	5.8	5.7
N	4.9	4.5	4.0	3.6	3.1	2.7	2.2	1.8	1.3	0.9	0.4
O	29.8	30.5	31.2	31.8	32.5	33.2	33.9	34.6	35.2	35.9	36.6
S	0.5	0.4	0.4	0.3	0.3	0.2	0.2	0.2	0.1	0.1	0.0
Cl	0.7	0.6	0.5	0.5	0.4	0.3	0.3	0.2	0.2	0.1	0.0

Table 2. Ash Composition

	RC	10 wt % bark	20 wt % bark	30 wt % bark	40 wt % bark	50 wt % bark	60 wt % bark	70 wt % bark	80 wt % bark	90 wt % bark	bark
content of bark ash in total fuel ash (%)	0	7	14	22	30	40	49	60	72	85	100
elemental analysis (wt % db)											
P	1.29	1.17	1.04	0.92	0.80	0.67	0.55	0.42	0.30	0.17	0.05
Si	0.05	0.09	1.30	0.17	0.21	0.26	0.30	0.34	0.38	0.42	0.46
Al	0.01	0.01	0.02	0.03	0.04	0.05	0.06	0.07	0.08	0.09	0.10
Mg	0.42	0.38	0.35	0.31	0.28	0.25	0.21	0.18	0.15	0.11	0.08
Ca	0.79	0.81	0.83	0.84	0.86	0.88	0.90	0.91	0.93	0.95	0.96
Na	0.45	0.41	0.37	0.33	0.29	0.24	0.20	0.16	0.12	0.08	0.04
K	1.26	1.16	1.05	0.95	0.84	0.74	0.64	0.53	0.43	0.32	0.22
Mn	0.01	0.01	0.01	0.02	0.02	0.03	0.03	0.04	0.04	0.04	0.05
Fe	0.02	0.02	0.03	0.03	0.03	0.04	0.04	0.04	0.04	0.05	0.05
Ti	0.00	0.00	0.00	0.00	0.00	0.00	0.00	0.00	0.00	0.00	0.00
Zn	0.00	0.00	0.00	0.00	0.00	0.00	0.01	0.01	0.01	0.01	0.01

**Figure 4.** Elemental average composition of fly ash samples obtained by SEM/EDX on a carbon- and oxygen-free basis.

simple statistical analysis was used to infer prevailing agglomeration mechanisms (see section 3.6).

3.4. Composition of the Layer on Bed Material Particles before the Agglomeration Stage. The composition of the layer on the bed material particles after combustion was studied using SEM/EDX (Figures 7 and 8). Two different compositions for the layers could be distinguished, as reported by other researchers.²⁵

An inner reaction layer (Figure 7) is present in the samples from the combustion of fuel mixtures having 30 wt % bark or more. It is composed of potassium, sodium, calcium, and silicon (mainly from the bed particles), in a composition that is similar for all the fuel mixtures and consistent with the composition of the inner reaction layer found for bark in other studies.^{16,25} This layer mainly consists of potassium silicates, whose first melting point could be as low as 750 °C; its presence indicates the inward attack of potassium compounds on the quartz sand. Further incorporation of calcium compounds into the melt takes place at a later stage.²⁶ The transport of potassium to the silica bed grains is expected to occur via the direct reaction of bed material with gaseous and/or aerosol alkali compounds.²⁵ When fuels with a high alkali metal and phosphorus content are fired, potassium phosphates may react with silica bed particles.³¹ The formation of an inner reaction layer may be followed by the formation of an outer layer that is rich in calcium. This layer is expected to prevent the further reaction of potassium with the bed grains^{17,27,31} and further depolymeriza-

tion of the silicates.²⁷ The first melting point of calcium silicate is higher than that of potassium silicate, so agglomeration in the FBC environment could be prevented if a calcium-rich coating formed around the silica grains.

The composition of the outer layer (Figure 8) exhibits trend similar to that of fly ash (Figure 4). As the proportion of bark in the fuel mixture increases, the calcium content increases, while phosphorus and potassium exhibit a decreasing trend. It has been suggested that the formation of the outer coating layer proceeds according to the following mechanisms: fine ash particles are entrapped by the molten silicate (the inner reaction layer) on the surface of the bed material particles,²⁶ or may be deposited via the direct adhesion of molten fuel ash particles.³⁵ The latter could occur when particles are still burning, as discussed in other studies.^{24,36} In the fuel mixtures with 60 wt % bark and higher, calcium became the dominant element in the outer layer. At the other extreme, for 100 wt % RC and the mixture with only a small amount of bark (10 wt %), the outer coating layer is dominated by phosphates. These observations indicate that the adhesion of sticky fuel ash particles may be the main mechanism underlying layer formation.

It is assumed that comparing the compositions of the layers with those of the agglomerate necks will make it possible to identify the layer responsible for agglomerate formation.

3.5. Agglomeration Tendency of Mixtures of Rapeseed Cake and Bark. The agglomeration tendency of mixtures of rapeseed cake and bark was determined using controlled fluidized-bed agglomeration tests. The initial defluidization temperatures (IDT) and the total defluidization temperature (TDT), described in section 2.4, were plotted as functions of the mixture composition (Figure 9). An inaccuracy of ± 30 °C was determined in previous studies⁴¹ and is included in the figure. Rapeseed cake showed a strong agglomeration tendency, and total defluidization occurred during the combustion stage (800 °C). At the other extreme, the TDT for bark was >1045 °C, so it could not be measured due to the limitations of the experimental setup. These results are in agreement with findings from previous studies on the agglomeration tendency of bark.^{16,39} Figure 9 plots the TDT, which indicates the temperature at which the formation of agglomerates leads to the complete collapse of the bed and loss of fluidization. Also indicated is the initial defluidization temperature, the temperature at which the growth of agglomerates and/or slagging begin to occur. The IDT in this

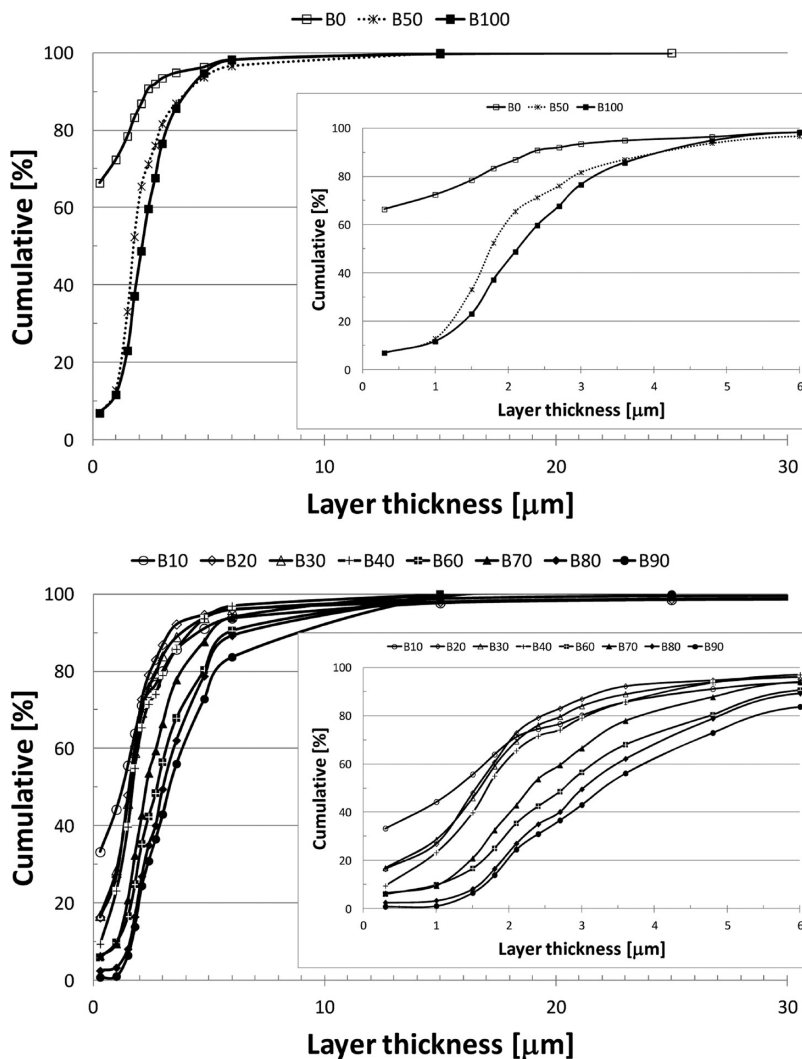


Figure 5. Cumulative distribution of the layer thickness on the bed material particle.

study was sometimes as much as 200 °C lower than the total defluidization temperature.

The defluidization temperature of the fuel mixtures increases with increasing proportion of bark. However, this trend is nonlinear for both the TDT and the IDT, which suggests that

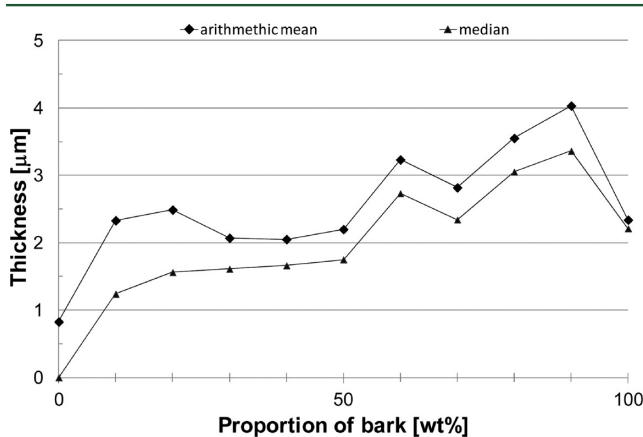


Figure 6. Arithmetic mean and median of the layer thickness data for the collected measurements versus the proportion of bark in the fuel mixture.

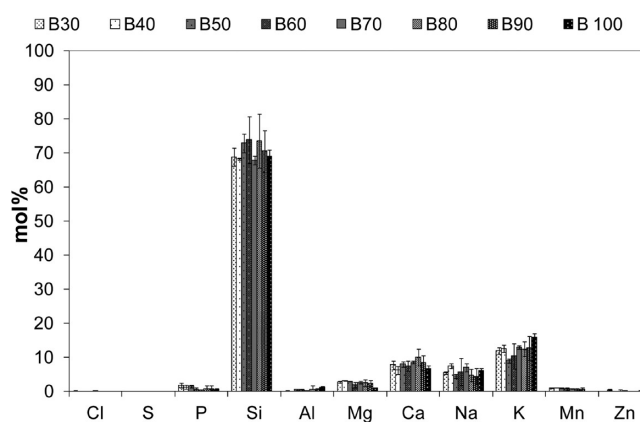


Figure 7. Average elemental composition of bed particle inner reaction layer on a carbon- and oxygen-free basis.

different agglomeration mechanisms may be involved, depending on the fuel mixture composition. The change in the trend in the graph of the TDT seems to occur between 20 and 30 wt % bark, whereas for IDT, it occurs in mixtures with 60 wt % bark. For mixtures dominated by RC ash (0–50 wt % bark), a constant decline in the pressure curve can already be observed during the combustion stage (800 °C). Accordingly, it is

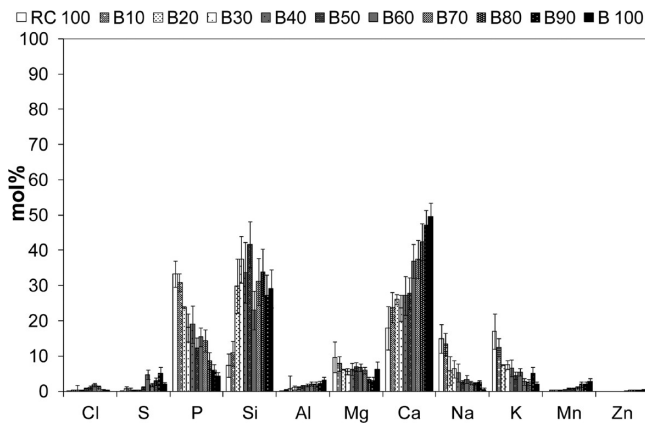


Figure 8. Average elemental composition of bed particle outer coating layer on a carbon- and oxygen-free basis.

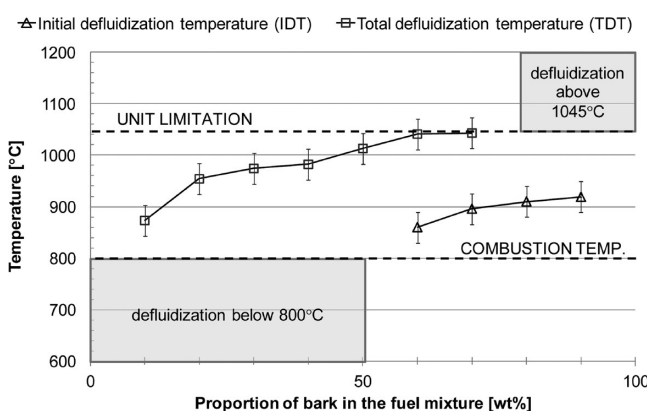


Figure 9. Defluidization temperatures versus proportion of bark in the fuel mixture.

reasonable to suppose that initial defluidization occurs during combustion.

From Figure 10, it is apparent that there is a correlation between the molar ratios, the defluidization temperatures, and the formation of an inner reaction layer.

Four molar ratios were plotted as functions of the fuel mixture composition. The Ca/P molar ratio for 60 wt % bark is >1.2 , and the molar ratio of alkali metals to alkaline-earth metals is 0.8. These molar ratios probably explain the trends seen in the defluidization curves. They indicate that the

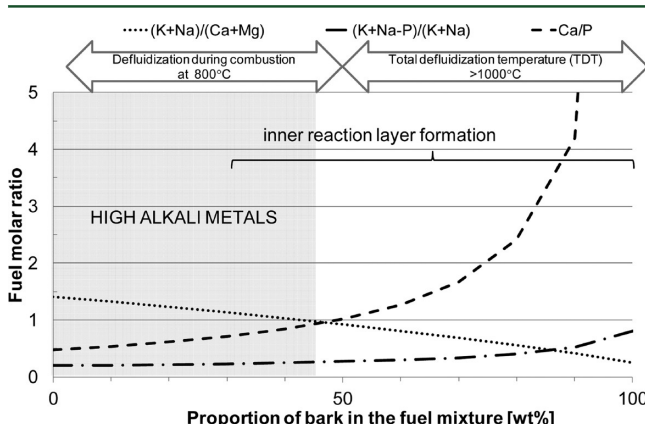


Figure 10. Fuel molar ratios versus proportion of bark in the fuel mixture.

reactions favor the formation of phosphates with a higher content of alkaline-earth metals than of alkali metals. The increased Ca content in a Ca–K–P system may shift the first melting temperature to over 1000 °C,¹⁵ which is consistent with the defluidization temperature for the mixture with 60 wt % bark ($TDT \approx 1045$ °C). In addition to the Ca/P and $(Na+K)/(Ca+Mg)$ molar ratios, the $(K+Na-P)/(K+Na)$ molar ratio is plotted; it indicates the amount of alkali metals that may be available for the formation of alkali silicates, alkali chlorides, or alkali sulfates. The strong affinity of phosphorus for alkali metals was reported by Boström et al.,¹⁴ and alkali-metal phosphates are formed preferentially if both silicon and phosphorus are present. The molar ratio $(K+Na-P)/(K+Na)$ was below 0.3 for mixtures with up to 60 wt % bark. An inner reaction layer was observed in mixtures with as little as 30 wt % bark. In such mixtures, the molar ratio of available alkali metals is similar to that for 100 wt % rapeseed cake combustion (below 0.25), indicating that alkali phosphates may be reacting with silica bed particles (Figure 10), as suggested by Barišić et al.³¹

3.6. Agglomerates. Figure 11–14 present SEM/EDX analyses of the agglomerates. For pure bark combustion (Figure 11), the composition of the neck formed between two bed material particles resembles that of the inner reaction layer. Agglomeration of the bed material occurs via the formation of a molten potassium silicate layer, i.e., an inner reaction layer.²⁵ The reaction between the silica bed material particles and the ash-forming elements originating from the fuel, which leads to layer formation, is the dominant mechanism underlying agglomerate formation. This mechanism can be described as a reactive mechanism. In the case of 100 wt % RC, the direct adhesion of partly molten ash particles to bed particles could be the driving force for the formation of agglomerates. Since no chemical interaction was observed between the bed material particles and the molten ash, this mechanism is considered to be a nonreactive mechanism. It is similar to the mechanisms described by De Geyter et al.,³⁷ under the assumption that no chemical reaction occurs between the bed material particle and the molten fuel ash. The composition of the necks in the agglomerates indicates the presence of two main phases, K–Mg–P and Ca–K–Na–P (Figure 11). The formation of these two types of phosphates is consistent with findings from studies on the agglomeration of phosphorus-rich fuels.¹⁶ It has been suggested that agglomeration during the combustion of rapeseed meal can be attributed to the formation of partially molten Mg–K–P and Ca–K–P. In this study, because of the high sodium content of rapeseed cake, the combustion of 100 wt % RC results in the formation of the calcium phosphates rich in sodium.

Figure 12 shows the composition of fuel ash particles that glue together two silica sand particles; the particles came from 10 wt % bark, and their composition is similar to that of the necks formed after the combustion of 100 wt % RC (Figure 11). The composition of the necks formed between silica grains after the combustion of other fuel mixtures is shown in Figures 13 and 14. Here, the agglomerates could be the result of the silicate layers that formed on the bed particles, but they could also be attributed to the formation of sticky fuel ash particles, suggesting a mixed agglomeration mechanism (reactive and nonreactive mechanisms). The potassium silicate matrix is formed with embedded phosphates. As the proportion of bark increased, the content of alkali metals associated with phosphorus within the silicate matrix decreased. This trend is

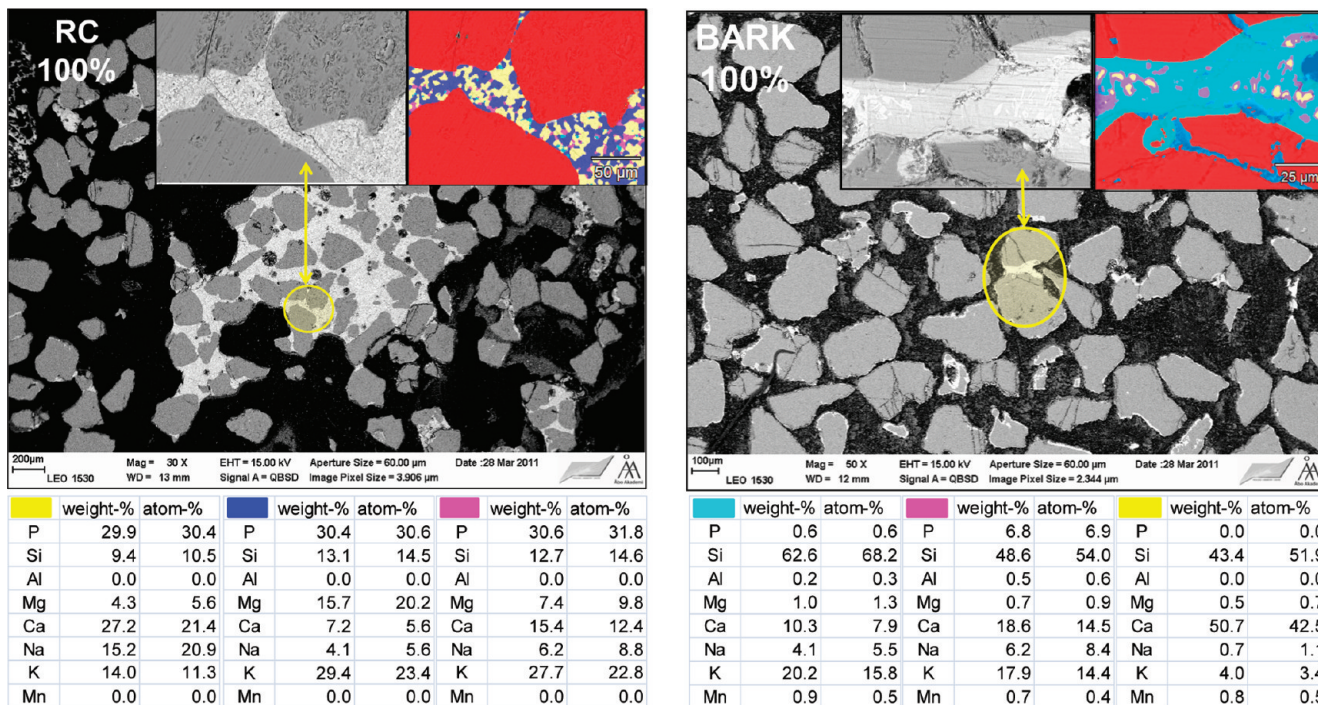


Figure 11. Agglomerates from rapeseed cake (RC) (left) and bark (right).

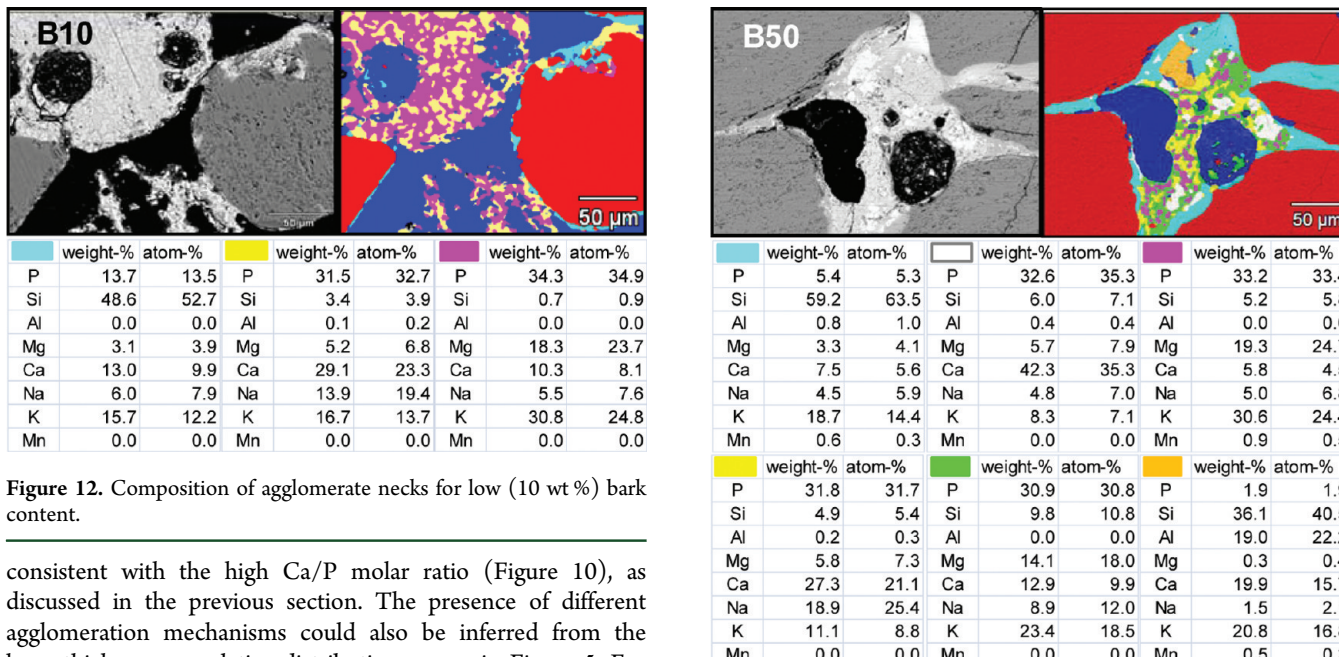


Figure 12. Composition of agglomerate necks for low (10 wt %) bark content.

consistent with the high Ca/P molar ratio (Figure 10), as discussed in the previous section. The presence of different agglomeration mechanisms could also be inferred from the layer thickness cumulative distribution curves in Figure 5. For 100 wt % RC, the cumulative distribution of the layer thickness around the particles indicates that there is almost no layer formation, so the nonreactive mechanism is responsible for agglomeration. For 100 wt % bark, a uniform layer was observed; therefore, in this case, the reactive mechanism is responsible for agglomeration. For mixtures with low proportions of bark (10–40 wt %), which corresponds to more than 20% of the thickness measurements below 1 μm and more than 60% below 2 μm), the dominant mechanism seems to be the nonreactive mechanism, since either a nonuniform layer or no layer at all was observed around the particle grains. For mixtures with 60 wt % bark and higher, there was a uniform layer around the silica grains, suggesting that the reactive

Figure 13. Composition of agglomerate necks for 50 wt % bark.

mechanism is dominant. What is interesting is the layer thickness distribution for 50 wt % bark. This type of layer could be produced by either the reactive and nonreactive mechanism based on the description of the groups in section 3.3, making it impossible to determine which mechanism is dominant.

4. CONCLUSIONS

Mixtures of rapeseed cake (RC), which is a phosphorus-rich fuel, and bark, ranging from 0 to 100 wt % bark, were systematically studied. The initial defluidization temperature (IDT) and total defluidization temperature (TDT) were

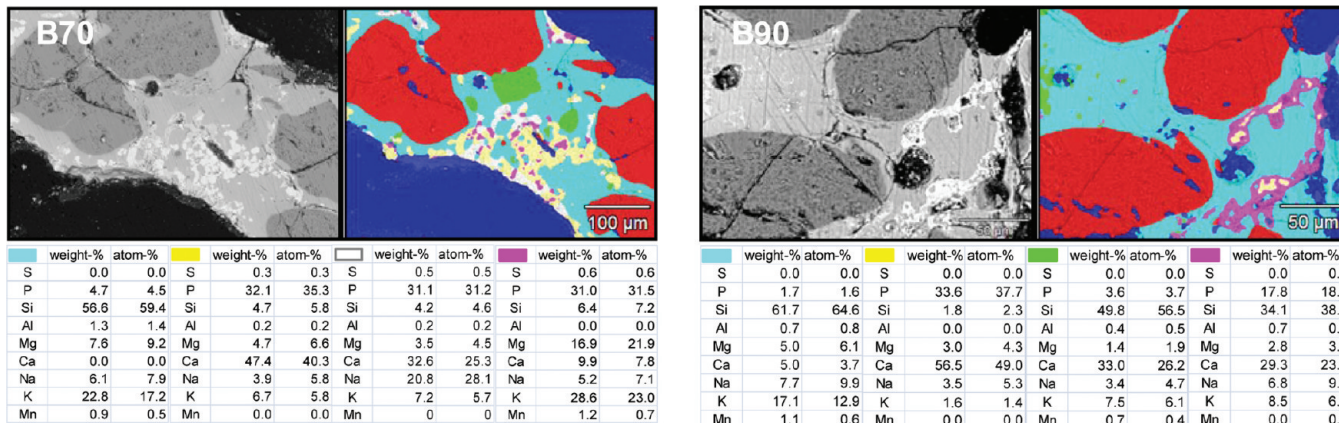


Figure 14. Composition of agglomerate necks for mixtures with high bark content: 70 wt % (left) and 90 wt % (right).

determined for the mixtures in a bench-scale bubbling fluidized-bed reactor under controlled conditions.

The IDT for mixtures containing up to 50 wt % bark was as low as the combustion temperature (800 °C). As the proportion of bark increased, the defluidization temperature increased. Mixtures with a minimum of 60 wt % bark resulted in significantly increased defluidization temperatures and reduced bed agglomeration tendencies, compared to that which occurs in RC monocombustion. This could be understood in terms of the following molar ratios: a Ca/P ratio of >1.27 and an (Na+K)/(Ca+Mg) ratio of <0.8.

The agglomeration mechanisms for these two fuels and mixtures of them are related to their ash-forming matter, resulting in different patterns of layer formation and different bed agglomeration mechanisms. During RC combustion, a discontinuous bed particle layer was observed that has the appearance of molten ash glued to the silica sand particles. During bark combustion, a continuous layer ~3 μm thick formed, consisting of both an inner reaction and an outer coating layer. From the distribution of the layer thickness around the bed material particles, it was possible to identify the dominating mechanism underlying bed agglomeration. It was found that in mixtures containing 40 wt% and less bark, the nonreactive mechanism prevails. In mixtures containing at least 60 wt % bark, the reactive mechanism prevails. In the mixture with 50 wt % bark, there is evidence that both mechanisms may play a role in bed agglomeration.

Investigations of the agglomerate neck composition during the combustion of 100 wt % RC revealed that the partly molten ash found between the silica sand particles consisted mainly of phosphates: magnesium–potassium phosphates, and calcium–potassium/sodium phosphates. Because of the high sodium content of RC, the combustion of 100 wt % RC results mainly in the formation of sodium–calcium phosphates. Although there are indications that the phosphates react with the silica bed particles, the precise form of the phosphates involved remains undetermined.

The results show that it may be possible to burn up to 40 wt % RC with bark without encountering low defluidization temperatures. However, combustion experiments of longer duration should be carried out, and investigation of other ash-related problems should be investigated before large-scale application.

AUTHOR INFORMATION

Corresponding Author

*E-mail: ppiotrow@abo.fi.

Notes

The authors declare no competing financial interest.

ACKNOWLEDGMENTS

The financial support provided by the Graduate School in Chemical Engineering (Finland) and by FUSEC, a project funded mainly through National Technology Agency of Finland (TEKES) and scientifically coordinated by the Process Chemistry Centre at Åbo Akademi University, Turku, Finland, is acknowledged. Financial support from the Swedish Research Council (VR) is also highly appreciated. Dr Andrzej Grzybowski (Czestochowa University of Technology–Institute of Mathematics) is thanked for sharing his expertise in statistics. Linus Silvander (Åbo Akademi–Process Chemistry Center) is acknowledged for SEM/EDX analyses. Continuous support during combustion experiments of Ulf Nordström (Umeå University–Energy and Technology and Thermal Process Chemistry) is highly appreciated.

REFERENCES

- Jenkins, B. M.; Baxter, L. L.; Miles, T. R. Jr; Miles, T. R. *Fuel Process. Technol.* **1998**, *54*, 17–46.
- Vassilev, S. V.; Baxter, D.; Andersen, L. K.; Vassileva, C. G. *Fuel* **2010**, *89*, 913–933.
- Tortosa Masiá, A. A.; Buhre, B. J. P.; Gupta, R. P.; Wall, T. F. *Fuel Process. Technol.* **2007**, *88*, 1071–1081.
- Petersson, A.; Zevenhoven, M.; Steenari, B. M.; Åmand, L. E. *Fuel* **2008**, *87*, 3183–3193.
- Piotrowska, P.; Zevenhoven, M.; Davidsson, K.; Hupa, M.; Åmand, L.-E.; Barišić, V.; Coda Zabetta, E. *Energy Fuels* **2010**, *24*, 4193–4205.
- Hupa, M. *Energy Fuels* **2012**, *26*, 4–14.
- Baxter, L. L.; Miles, T. R.; Miles, T. R. Jr.; Jenkins, B. M.; Milne, T.; Dayton, D.; Bryers, R. W.; Oden, L. L. *Fuel Process. Technol.* **1998**, *54*, 47–78.
- Hiltunen, M.; Barišić, V.; Åmand, L.-E.; Coda Zabetta, E. Combustion of different types of biomass in CFB boilers. Presented at the *16th European Biomass Conference*, Valencia, Spain, June 2008.
- Hupa, M. *Fuel* **2005**, *84*, 1312–1319.
- Coda Zabetta, E.; Barišić, V.; Peltola, K.; Hotta, A. Foster Wheeler Experience with biomass and waste in CFBs. In *Proceedings of the 33rd Clearwater Conference*, Clearwater, FL, USA, June 2008.
- Werther, J.; Saenger, M.; Hartge, E.-U.; Ogada, T.; Siagi, Z. *Prog. Energy Combust. Sci.* **2000**, *26*, 1–27.

- (12) Frandsen, F. J. *Fuel* **2005**, *84*, 1277–1294.
- (13) Theis, M.; Skrifvars, B. J.; Hupa, M.; Tran, H. *Fuel* **2006**, *85*, 1125–1130.
- (14) Boström, D.; Skoglund, N.; Grimm, A.; Boman, C.; Öhman, M.; Broström, M.; Backman, R. *Energy Fuels* **2012**, *26*, 85–93.
- (15) Lindström, E.; Sandström, M.; Boström, D.; Öhman, M. *Energy Fuels* **2007**, *21*, 710–717.
- (16) Grimm, A.; Skoglund, N.; Boström, D.; Öhman, M. *Energy Fuels* **2011**, *25*, 937–947.
- (17) Piotrowska, P.; Zevenhoven, M.; Davidsson, K.; Hupa, M.; Åmand, L.-E.; Barišić, V.; Coda Zabetta, E. *Energy Fuels* **2010**, *24*, 333–345.
- (18) Nevalainen, H.; Leino, T.; Tourunen, A.; Hiltunen, M.; Coda Zabetta, E. Deposits and emissions during the co-combustion of biodiesel residue with coal and biomass in a CFB pilot. In *Proceedings of the 9th International Conference on Circulating Fluidized Beds*, Hamburg, Germany, May 2008.
- (19) Hao, W.; Castro, M.; Jensen, P. A.; Frandsen, F. J.; Glarborg, P.; Dam-Johansen, K.; Røkke, M.; Lundtorp, K. *Energy Fuels* **2011**, *25*, 2874–2886.
- (20) Pontoppidan, K.; Pettersson, D.; Sandberg, A.-S. *Anim. Feed Sci. Technol.* **2007**, *132*, 137–147.
- (21) Siegell, J. H. *Powder Technol.* **1984**, *38*, 13–22.
- (22) Öhman, M.; Nordin, A.; Skrifvars, B. J.; Backman, R.; Hupa, M. *Energy Fuels* **2000**, *14*, 169–178.
- (23) Olofsson, G.; Ye, Z.; Bjerle, I.; Andersson, A. *Ind. Eng. Chem. Res.* **2002**, *41*, 2888–2894.
- (24) Lin, W.; Dam-Johansen, K.; Frandsen, F. *Chem. Eng. J.* **2003**, *96*, 171–185.
- (25) Brus, E.; Öhman, M.; Nordin, A. *Energy Fuels* **2005**, *19*, 825–832.
- (26) Zevenhoven-Onderwater, M.; Öhman, M.; Skrifvars, B. J.; Backman, R.; Nordin, A.; Hupa, M. *Energy Fuels* **2006**, *20*, 818–824.
- (27) De Geyter, S.; Öhman, M.; Boström, D.; Eriksson, M.; Nordin, A. *Energy Fuels* **2007**, *21*, 2663–2668.
- (28) Bartels, M.; Lin, W.; Nijenhuis, J.; Kapteijn, F.; van Ommen, J. R. *Prog. Energy Combust. Sci.* **2008**, *34*, 633–666.
- (29) Scala, F.; Chirone, R. *Biomass Bioenergy* **2008**, *32*, 252–266.
- (30) Davidsson, K. O.; Åmand, L.-E.; Steenari, B.-M.; Elléd, A.-L.; Eskilsson, D.; Leckner, B. *Chem. Eng. Sci.* **2008**, *63* (21), 5314–5329.
- (31) Barišić, V.; Åmand, L.-E.; Coda Zabetta, E. The role of limestone in preventing agglomeration and slagging during CFB combustion of high phosphorus fuels. Presented at *World Bioenergy*, Jönköping, Sweden, May 2008.
- (32) Carter, C. B.; Norton, M. G. *Ceramic Materials: Science and Engineering*; Springer: New York, 2007. (ISBN: 978-0-387-46270-7.)
- (33) Skrifvars, B. J.; Hupa, M.; Backman, R.; Hiltunen, M. *Fuel* **1994**, *73* (2), 171–176.
- (34) Visser, H. J. M.; van Lith, S. C.; Kiel, J. H. A. *J. Energy Resour.–ASME* **2008**, *130*, 011801–1–011801–6.
- (35) Brus, E. *Bed agglomeration during combustion and gasification of biomass fuels—mechanisms and measures prevention*. Licentiate Thesis, Energy Technology and Thermal Process Chemistry, Umeå University, 2004.
- (36) Scala, F.; Chirone, R.; Salatino, P. *Fuel Process. Technol.* **2003**, *84*, 229–241.
- (37) De Geyter, S. *Measures for preventing bed agglomeration using ash reaction chemistry*, Licentiate Thesis, Energy Technology and Thermal Process Chemistry, Umeå University, 2008.
- (38) Novaković, A.; van Lith, S. C.; Frandsen, F. J.; Jensen, P. A.; Holgersen, L. B. *Energy Fuels* **2009**, *23*, 3423–3428.
- (39) Eriksson, G.; Hedman, H.; Boström, D.; Petersson, E.; Backman, R.; Öhman, M. *Energy Fuels* **2009**, *23*, 3930–3939.
- (40) Boström, D.; Eriksson, E.; Boman, C.; Öhman, M. *Energy Fuels* **2009**, *23*, 2700–2706.
- (41) Öhman, M.; Nordin, A. *Energy Fuels* **1998**, *12*, 90–94.
- (42) Barišić, V.; Hupa, M. *Fuel* **2007**, *86*, 464–468.
- (43) Morey, G. W. *J. Am. Chem. Soc.* **1954**, *76* (18), 4724–4726.
- (44) Theis, M.; Skrifvars, B. J.; Zevenhoven, M.; Hupa, M.; Tran, H. *Fuel* **2006**, *85*, 1992–2001.
- (45) Dima, I. C.; Grzybowski, A. Z.; Grabara, J. K.; Goldbach, I. R.; Popescu, O. R. Utilizing of Mathematics—Statistics Methods Concerning Mechanic Properties of Heavy Steel Plates: Dealing with the Ill Conditioned Data. In *Proceedings of the International Conference on Mathematical Models for Engineering Science (MMES '10)*, Puerto De La Cruz, Tenerife, November/December 2010; Mladenov, V., Psarris, K., Mastorakis, N., Caballero, A., Vachtsevanos, G., Eds.; World Scientific and Engineering Academy and Society (WSEAS) Press: 2010; pp 277–284.